

The Design and Investigation of Hybrid a Microfluidic Micromixer

Muhammad Waqas ¹, Giedrius Janusas ¹, Vytenis Naginevičius ² and Arvydas Palevicius ^{1,*}

¹ Faculty of Mechanical Engineering and Design, Kaunas University of Technology, 51424 Kaunas, Lithuania; muhammad.waqas@ktu.edu (M.W.)

² Faculty of Applied Sciences, Kaunas University of Applied Engineering Sciences, 50155 Kaunas, Lithuania

* Correspondence: arvydas.palevicius@ktu.lt

Abstract: Today, microfluidics has become a revolutionary interdisciplinary topic with considerable attention in a wide range of biotechnology applications. In this research work, a numerical investigation of a microfluidic micromixer is carried out using a hybrid actuation approach with different micropillar shapes and gaps. For this purpose, COMSOL Multiphysics v.5.6. is used with three different physics, such as thermoviscous acoustic physics to solve acoustic governing equations, laminar physics to solve fluid flow governing equations, and diluted transport species to solve mixing governing equations. The simulations were carried out at different Reynolds numbers such as 2, 4, 6, 8, 10, and 12 with an oscillation frequency of 15 kHz. The results were in the form of acoustic characteristics such as acoustic pressure, acoustic velocity, acoustic stream, mixing index, and fluid flow behaviour at various Reynolds numbers. The results revealed that the inclusion of micropillars improved the mixing performance and strength of the acoustic field, resulting in an improvement of the mixing performance compared to the case without micropillars. In addition, the mixing performance is also investigated at different Reynolds numbers, and a higher mixing index is investigated at lower Reynolds numbers. Moreover, it was also investigated that blade-shaped micropillars with 0.150 mm gaps deliver the best results compared to the other cases, and the maximum and minimum values of the mixing index are 0.97 and 0.72, respectively, at Reynolds number 2. The main reason behind this larger mixing index at low Reynolds numbers is due to the inclusion of micropillars that enhance the diffusion rate and contact area, leading to the homogenisation of the heterogeneous fluids in the microchamber. The obtained results can be extremely helpful for the design and modifications of a hybrid microfluidics micromixer.

Keywords: micromixing; acoustic streaming; acoustofluidics; microfluidics; mixing index

Citation: Waqas, M.; Janusas, G.; Naginevičius, V.; Palevicius, A. The Design and Investigation of a Hybrid Microfluidic Micromixer. *Appl. Sci.* **2024**, *14*, 5315. <https://doi.org/10.3390/app14125315>

Academic Editor: Ricardo Castedo

Received: 29 May 2024

Revised: 14 June 2024

Accepted: 17 June 2024

Published: 19 June 2024



Copyright: © 2024 by the authors. Licensee MDPI, Basel, Switzerland. This article is an open access article distributed under the terms and conditions of the Creative Commons Attribution (CC BY) license (<https://creativecommons.org/licenses/by/4.0/>).

1. Introduction

Today, microfluidics has become a revolutionary interdisciplinary topic with considerable interest in a wide range of bioengineering applications such as mixing, sorting, separation, detection, and reaction [1]. Microfluidic devices are the best replica of a conventional lab due to their unique abilities, such as small sample consumption, and exact control of fluid particles on the microscale [2]. In addition, microfluidics have unique properties, such as high surface area to volume ratios and rapid mass and heat transfer, which have paved the way for innovations in a variety of scientific and commercial fields, promising increased efficiency, portability, and cost-effectiveness in a wide range of applications [3]. In microfluidic devices, the manipulation of fluid particles can be challenged through microchannels with dimensions ranging from micrometres to millimetres [4]. The high degree of mixing of biofluids and biochemicals is a crucial feature in many microfluidic devices, aiming to obtain a homogeneous mixture between two different heterogeneous components under laminar flow conditions with minimum fabrication com-

plexity [5]. Over the decades, numerous studies have been carried out, and several microfluidic micromixers have been proposed. Moreover, the extensive literature shows a wide categorisation of microfluidics micromixers into two major types, active and passive micromixers, based on the external energy supply to operate [6].

Active micromixers need external sources such as electric fields, acoustic fields, magnetic fields, and photothermal effects to operate and control the mixing fluids [7]. These sources cause disturbance in the flow fluid pattern, leading to the enhancement of heterogeneous fluid species transport [8]. Such a kind of disturbance enhances the interfacial area between two different heterogeneous fluids. In addition, the main advantages of using the active actuation approach are higher mixing, which is best suitable for precise control, and a complex mixing pattern for various biofluids and chemicals [9]. Some drawbacks are also studied, as the active actuation approach needs some external source or force that consumes power and requires more space and cost compared to the passive approach and can interfere with the chemical and biological properties of fluids [10]. Chandan Kumar et al. [11] developed a numerical model to simulate transportation phenomena in microfluidic systems with fluorescent and ferrofluid dye that was induced by the nonuniform magnetic source. Masoud Rahimi et al. [12] demonstrated the impact of ultrasound waves on the mixing performance of a type micromixer. They used piezoelectric transducers to generate vibrations. Habib Jalili et al. [13] examined the optimisation of effective parameters and their impact on mixing quality in a 2D active-type micromixer. Yanwen Gong et al. [14] investigated the concentration field and flow distribution in the microchannel and observed two different circulation flows and four various rotating vortices produced in the expansion micromixer chamber by inducing AC electric fields. Siyue Xiong et al. [15] proposed a novel type of rhombic electro-osmotic micromixer using the principles of both convergence and divergence with microelectrodes to enhance mixing performance. They examined the performance of the micromixer by changing the angle and the combination of various rhombic elements. Bappa Mondal et al. [16] numerically investigated the mixing and flow characteristics of a charged heterogeneous micromixer for an electro-osmotic flow with obstacles both in the top and bottom walls. Kasavajhula Naga Vasista et al. [17] examined the electro-osmotic mixing attributes of fluid flow by a hydrophobic microchannel with interfacial slips subjected to different surface charges. They also developed a theoretical framework to solve the Poisson–Boltzmann equation.

On the other hand, passive micromixers do not depend on any external energy source for fluid manipulation and actuation purposes [18]. In addition, the passive-type microfluidics micromixer is more reliable and robust because of its simplicity and cost-effectiveness [19]. In a passive mixer, the geometrical characteristics of the microchannel are utilised in many microfluidics systems due to its larger system stability [20]. Moreover, mass transfer is also dominated in the passive microfluidics system by molecular diffusion and convection shortening the diffusion paths [21]. Passive micromixers were used to create nanoparticles in continuous, batch, or semi-batch modes [22]. On the other hand, some disadvantages are also studied due to a lack of precise control; mixing efficiency is also limited in a passive-type micromixer, and there have been some design constraints to obtain higher mixing performance. Zhenghao Wang et al. [23] reported 3D PDMS microfluidics micromixers based on splitting–stretching and then recombined fluid streams in order to enhance diffusion that increases mixing with low Reynolds numbers. Yice Shao et al. [24] examined the impact of microchannel width, applied voltage, and waveform on fluid mixing and flow characteristics numerically and experimentally. They used a passive approach to investigate the mixing performance of a micromixer. Kevin Ward et al. [25] explored a novel approach to improve mixing within microfluidic devices for various applications. They also used ridges or slanted walls and varied the various geometrical configurations and patterns to evaluate the mixing performance of the microfluidic device using numerical simulations. Jae Bem You et al. [26] developed a Y-shaped turbulent microfluidics micromixer made of PDMS and glass substrate in order to investigate mixing performance using experimental and numerical approaches. Xueye Chen et al. [27] used

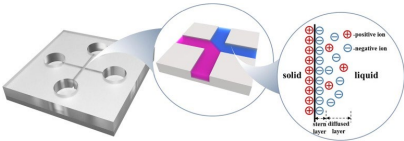
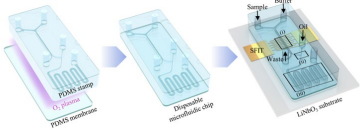
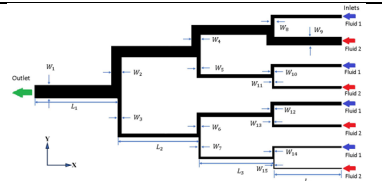
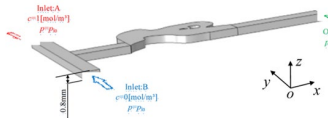

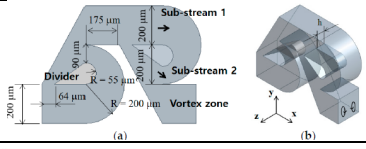
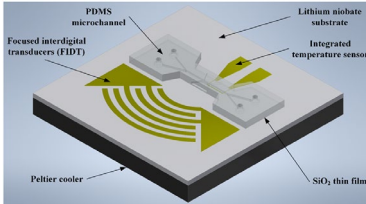
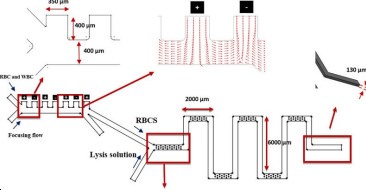
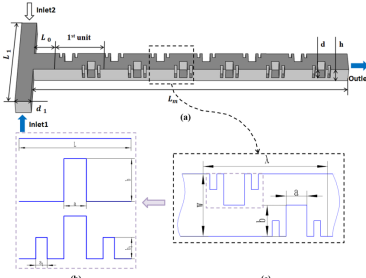
the fractal principle with a multi-objective genetic algorithm and multi-objective optimisation of the cantor fractal baffle microfluidics micromixer to investigate the mixing performance at different Reynolds numbers. Farahinia et al. studied the optimal design of the passive T-mixer, which involved the prescribed pattern of barriers and furrows with various geometrical configurations using a numerical approach. Min Xiong et al. [28] conducted a topology optimisation in order to enhance the mixing performance for microfluidic micromixers based on the Tesla valve principle.

Today, the acoustic wave-based approach has been widely applied in order to facilitate microfluidics due to its flexible control, short mixing distance, and intensive kinetic of biofluids [29]. Acoustic radiation and acoustic streaming are the two main phenomena that are used in microfluidics. The acoustic radiation force refers to the time-averaged force resulting from the time-harmonic nature of acoustic waves. On the other hand, the averaged flow produced by the non-linear interaction of the harmonic acoustic fields is known as acoustic flow [30]. In addition, some microstructures or microbubbles were added to the microchannel to improve acoustic mixing and mixing efficiency [31]. As a result, adaptable acoustic-facilitated micromixers have been used in a variety of domains, including materials synthesis, cell manipulation, and enzyme bioassay [32].

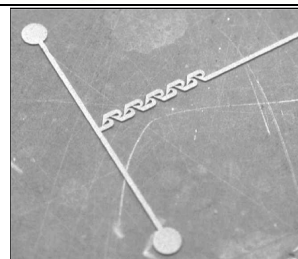
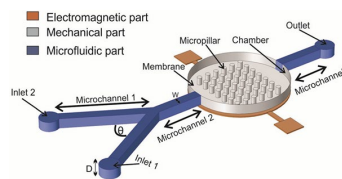
The mixing efficiency is an important parameter for measuring the proper mixing of heterogeneous biofluids and biochemicals [33]. There are several factors such as the total flow rate, the flow rate ratio, and other geometrical features that influence the mixing performance in microfluidics systems, although higher flow rates result in a shorter contact area in the microchannels and shorter mixing times [34]. On the other hand, a lower flow rate ratio might result in thinner layers that are wrapped by the sheath flow in a flow focus area and thus a shorter diffusion in lengths. Moreover, geometrical shapes in microfluidic channels are also influenced by mixing performance [35]. There are two common kinds of mixing geometry in passive microfluidics systems that greatly rely on the laminar diffusion mechanism, consequently limiting their mixing effectiveness. Most researchers have explored numerous geometrical modifications to enhance the interfacial area in order to increase and improve mixing performance [36]. Generally, two kinds of microchannels (T-shape and Y-shape) are widely used for mixing purposes in microfluidics systems. Fengli Liu et al. [37] proposed a new type of micromixer based on flexible artificial cilium that is actuated by a magnetic field. They used the cilium structure in a circular microchamber, which was then compared with pure diffusion, and observed that up to 80% of a 60 microlitre fluid in the chamber was fully mixed after 2 min under a magnetic flux of 22mT for 20 min. A more comprehensive literature review of the active and passive actuation approach is listed in Table 1.

Table 1. Summary of various micromixer designs.

Year	Goal	Microchannel Type	Microfluidic Type	Microchannel Design	References
2024	Development of a Tesla structure for efficient fluid mixing.	Tesla shape	Passive		[38]
2023	Development and characterisation of a 3D zig-zag microchannel.	3D zig-zag microchannel	Passive		[6]

2023	Investigate the impact of geometrical parameters and applied voltage on fluid mixing and fluid flow behaviour experimentally and numerically.	Cross-channel	Active		[24]
2023	Acoustic fluid approach to control the chemical concentration within picolitre droplets on a disposable microfluidic chip.	T-shape	Hybrid (Active and Passive)		[39]
2023	Investigation of fluid flow mixing in the fractal tree.	Fractal tree	Passive		[36]
2023	Micromixer topology optimisation based on a Tesla principle valve.	Tesla shape	Passive		[28]
2022	Development of a Tesla valve-based microfluidics micromixer.	Tesla shape	Passive		[40]
2022	Development of a Tesla-based micromixer with tip clearance.	Tesla shape	Passive		[41]
2022	Development and analysis of a microfluidics system with a thermal control unit to reduce thermal effects due to acoustic actuation.	Double Y-shape	Active		[8]
2022	Introduced a novel-type microfluidic microchannel design for sequential RBC separation and lysis.	Y-shape and zig-zag shape	Passive		[42]
2022	Investigation of different operational parameters by combining the fractal principle with the multi-objective genetic algorithm and the multi-objective optimisation of	Cantor fractal baffle shape micromixers	Passive		[27]

	cantor fractal baffle micromixers.		
2019	Design and optimisation of an active-based microchannel incorporated with micropillars.	Microchannel with micropillars	Hybrid (Active and Passive) [43]
2004	A novel in-plane passive microfluidic mixer with modified Tesla structures.	Tesla structure	Passive [44]



According to the current literature, it has been concluded that the actuation of fluid particles in microfluidic systems, especially for mixing applications, is necessary to improve the performance of the system. In addition, most of the authors used passive approaches, such as different geometrical configurations and parameters, to reduce the energy consumption and miniaturised microfluidics system. The authors have worked on different design configurations such as a Y-shape, a T-shape, a zig-zag, a circular chamber with micropillars, Tesla-based microchannels, cross-shape channels, cantor fractal baffle shape micromixers, a fractal tree shape with asymmetric microchannels, etc. On the other hand, some authors used active actuation approaches such as electromagnetic, acoustic, and photothermal to manipulate the fluid particles, especially for mixing applications. Moreover, it has also been examined that much less work has been conducted on the hybrid approach in which the combination of active and passive approaches is used for mixing applications. A hybrid microfluidic approach might offer numerous advantages to generate more versatile and efficient microfluidic systems, such as increasing the control and precision of the flowing fluid, reducing energy consumption, flexibility, and versatility, enhancing mixing performance, etc. In addition, the hybrid microfluidics micromixer may effectively solve the backflow issues and achieve robust backflow-free micromixing due to its precise mixing control, making this study more attractive in the point-of-care testing (POCT) application. Thus, there is great potential exists in using a hybrid approach in the design, development, and research of microfluidic systems for controlling and manipulating fluid particles, especially for mixing applications.

The main objective of this research work is to numerically evaluate the mixing performance of the microfluidic micromixer with different micropillar shapes and different micropillar gaps using the hybrid actuation approach. The nature of acoustic streaming velocity, acoustic velocity, and acoustic pressure were also investigated in the presence of micropillars with different gaps at different Reynolds numbers. Subsequently, based on these characteristics, mixing performance was evaluated due to acoustic streaming and its impact on species transport. The findings from this study also demonstrated how the proposed hybrid microfluidic micromixer can enhance the mixing index between two different heterogeneous species. The results obtained in this study can be extremely helpful for the design and modifications of microfluidic micromixers for the high-quality mixing of fluids.

2. Materials and Methods

This section describes the research scheme in which three different stages are developed to carry out current research work. In the first stage, a selection of conceptual designs of microfluidic micromixers is finalised with suitable geometrical features. The schematic

diagrams of four different microfluidics micromixer designs are shown in Figure 1. In the second stage, numerical simulations are performed using a hybrid actuation approach based on chosen micromixer designs. In the third stage, findings from numerical simulations are analysed and compared with previous studies for validation purposes.

2.1. Micromixer Design and Performance Parameters

Figure 1 describes the four different designs of microfluidic micromixers with geometrical features. The four geometries are differentiated by different micropillar shapes inside the microchamber. Figure 1a is a plane micromixing chamber with no micropillars. Figure 1b represents a micromixing chamber with circular-shaped micropillars that increase the acoustic streaming, leading to higher mixing performance. Similarly, Figure 1c represents the third micromixer design with hexagonal-shaped micropillars that help to attain a homogeneous mixing of two different heterogeneous fluid components at laminar flow conditions. Figure 1d represents the fourth micromixer design with blade-shaped micropillars that generate more vortices around the walls of the micropillars. The edges of blade-shaped micropillars help to increase the mixing performance of two different heterogeneous fluids.

However, the performance of the micro-mixer is measured in terms of the mixing index and concentration of two different heterogeneous fluid components at the outlet of the micromixer. The mixing index is measured based on the statistical approach. It is determined at any cross-section of the microchannel width from the concentration of the standard deviation of the heterogeneous fluid species using the following relation [23]:

$$M = 1 - \sqrt{\frac{\sigma^2}{\sigma_{\max}^2}} \quad (1)$$

$$\sigma = \sqrt{\frac{1}{n} \sum_{i=1}^n (c_i - \bar{c})^2} \quad (2)$$

$$\sigma_{\max} = \sqrt{\bar{c}(1 - \bar{c})} \quad (3)$$

where σ is the standard deviation, c_i is the concentration species of two different heterogeneous fluids, \bar{c} is the mean concentration of two different heterogeneous fluids, and σ_{\max} is the value of the maximum standard deviation of the two various species of heterogeneous fluids at a specified cross-section of the micromixer channel.

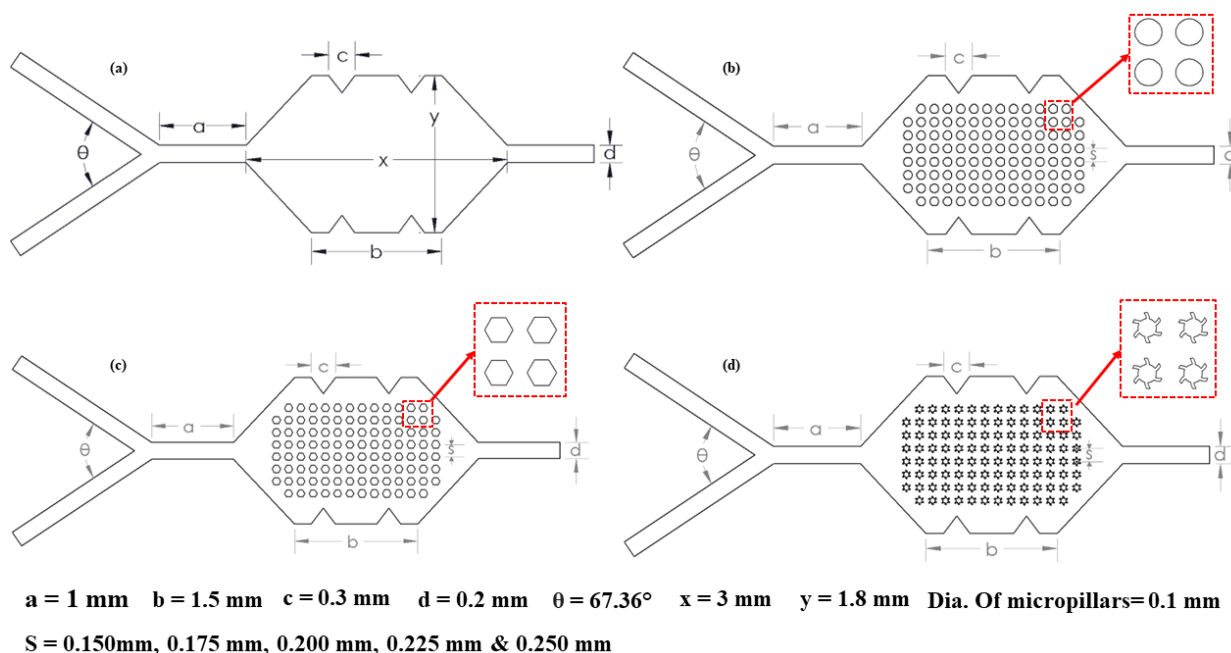


Figure 1. Four different geometries of micromixers: (a) plane-mixing chamber; (b) mixing chamber with circular micropillars; (c) mixing chamber with hexagonal micropillars; and (d) mixing chamber with blade-type micropillars.

2.2. Computational Domain and Meshing

In this research work, numerical simulations of four different micromixer designs are carried out to investigate the mixing performance using the hybrid actuation approach. The numerical scheme is used to solve the 2D computational domain of the micromixer, which has three microchannels, two inlets, one outlet, and one mixing chamber containing micropillars, as shown in Figure 2. The blue and red arrows indicate two different liquids and the green arrow indicates mixed liquid in the outlet. For numerical simulations, COMSOL Multiphysics is used. Furthermore, the meshing of micromixer models is also performed using COMSOL Multiphysics, as shown in Figure 3. The observed total number of elements and nodes are 47,057 and 24,893, respectively. The overall mesh quality lies in an acceptable range.

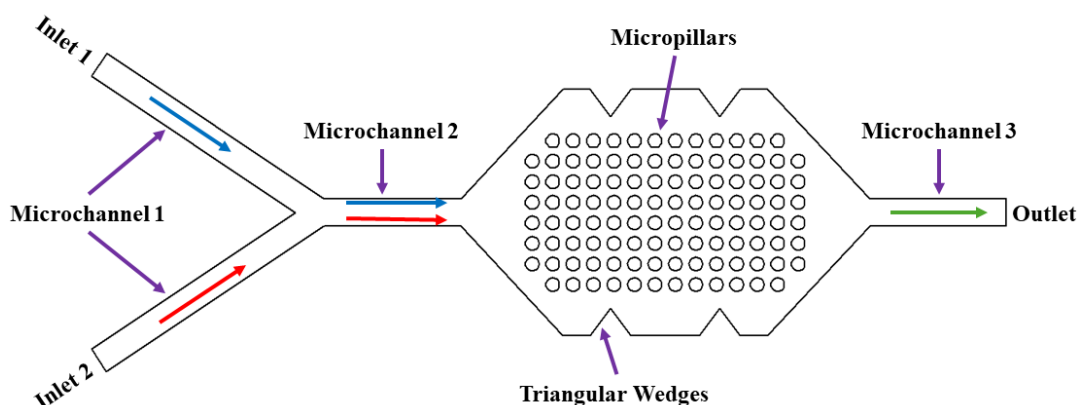


Figure 2. Two-dimensional computational domain for numerical simulations.

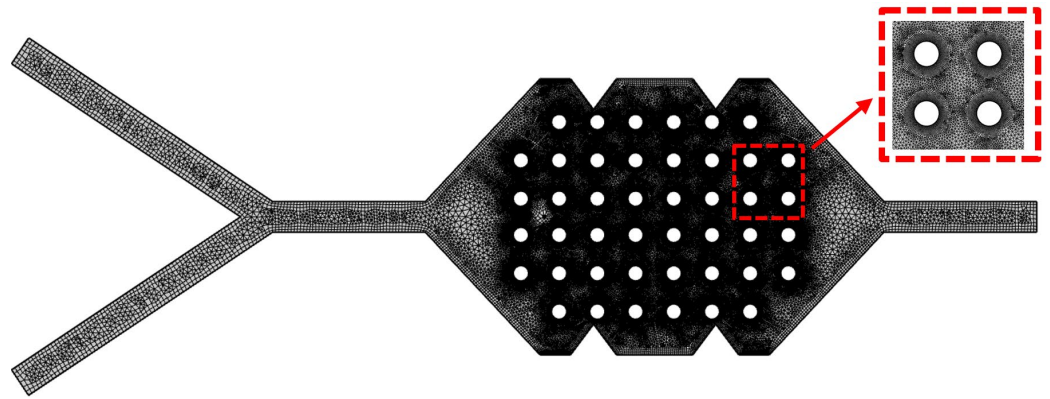


Figure 3. Micromixer mixing for numerical simulations.

2.3. Mathematical Modelling

Mathematical modelling generally describes the behaviour of acoustic phenomena and their interaction with flowing fluids in an acoustic mixing inside the microchannels. Acoustic mixing is a technique that uses acoustic waves to generate motion in the flowing fluid. In this section, a detailed description and mathematical relations of governing equations needed for the simulation of acoustic mixing are discussed. The governing equations related to mass and momentum conservation, such as the continuity equation and the Navier–Stokes equation, are described, respectively. In addition, there are three different numerical models: the thermoviscous acoustic model in which governing equations are obtained from linearised Navier–Stokes equations and can be used to solve continuity and momentum in the microchannels, the laminar flow model that solves the flow governing equations, and the transport-diluted species model that is used to determine mixing index. Furthermore, the boundary conditions applied on the micromixer have also been elaborated.

2.3.1. Mass and Momentum Conservation

The governing equations related to mass and momentum conservation, such as the equation of continuity and the Navier–Stokes equations for compressible Newtonian fluids, are given below [45].

$$\frac{\partial \rho}{\partial t} + \nabla \times (\rho v) = 0 \quad (4)$$

$$\rho \frac{\partial v}{\partial t} + \rho(v \times \nabla)v = -\nabla p + \mu \nabla^2 v + \beta \mu \nabla(\nabla \times v) \quad (5)$$

where ρ is the fluid density, μ is the dynamic viscosity of the fluid, β represents the viscosity ratio, p and v describes the pressure and velocity of the flowing fluid, respectively.

2.3.2. Thermoviscous Acoustic Model

The thermoviscous acoustic model generally describes the behaviour of acoustic waves with flowing fluids considering both viscous and thermal effects. This model plays an important role in predicting the behaviour of acoustic waves accurately in a system where viscous and thermal effects are involved. The thermoviscous acoustic model is useful for solving coupled partial differential equations, such as the Navier–Stokes equation for flowing fluid coupled with the governing equations, which involved heat conduction and acoustic wave equations. The governing equations for the thermoviscous acoustic model in the frequency domain are given below [46].

$$i\omega\rho_t + \nabla \times (\rho_o u_t) = 0 \tag{6}$$

$$i\omega\rho_o u_t = \nabla \times \rho_o \tag{7}$$

$$\sigma = -\rho_t 1 + \mu(\nabla u_t + (\nabla u_t)^T) - (\frac{2}{3}\mu - \mu_B)(\nabla \times u_t) 1 \tag{8}$$

$$\rho_t = \rho_o 1(\beta_T p_t - \alpha_p T_t) \tag{9}$$

$$\rho_t = p + p_b, \quad u_t = u + u_b, \quad T_t = \frac{\alpha_p T_o}{\rho_o C_p} p + T_b \tag{10}$$

where ω is natural frequency, μ represents the dynamic viscosity, u_t is wave velocity, T describes the fluid temperature, C_p is the specific heat capacity at a constant pressure, β_T describes the compressibility of the fluid at a constant temperature, and α_p is the coefficient of thermal expansion.

2.3.3. Laminar Model

The laminar model represents a mathematical approach that is used to describe the behaviour of flowing fluid in a laminar condition. The governing equations related to the laminar model are given below [47].

$$\rho(u \times \nabla)u = \nabla \times [-p 2 1 + K] + F \tag{11}$$

$$\rho \nabla \times u = 0 \tag{12}$$

where K describes the thermal effect in the force of the flowing fluid and F is the external volume exerted in the fluid.

2.3.4. Transport-Diluted Species Model

The transport-diluted species model is generally used to describe the mixing of two different chemically active species. In this work, the transport-diluted species model is used to solve the advection–diffusion equations after considering the consumption rate and production of reactants and products, respectively. The governing equations for the transport of diluted species in the frequency domain are given below [48].

$$\nabla \times j_i + u \times \nabla c_i = R_i \tag{13}$$

$$j_i = -D_i \nabla c_i \tag{14}$$

Here, c is the concentration of species, D is the diffusion coefficient, R represents the reaction rate for the reactant species, and j is the mass flux factor that describes the diffusive flux vector.

2.4. Numerical Scheme and Boundary Conditions

In this work, numerical simulations of hybrid microfluidics micromixers are carried out, and governing equations are solved using the finite element method (FEM) in COMSOL Multiphysics. A detailed description of the numerical methodology is shown in Figure 4. There are three different schemes, such as the thermoviscous acoustic scheme that is used to solve acoustic-related equations, the laminar scheme that is used to solve fluid flow equations with laminar behaviour, and the transport-diluted species scheme that is used to determine the mixing performance of the system. The walls of the microchannel were assumed to be solid walls and stationary with no slip and zero velocity conditions.

Thus, the flowing fluid at both inputs is assumed to be fully developed and uniform with a volumetric flow rate of 5 $\mu\text{L}/\text{min}$ and an oscillation frequency of 15 KHz. Moreover, simulations of the optimum micromixer design are also carried out at different Reynolds numbers to examine the flow behaviour inside the microchamber. The pressure boundary condition is set to zero at both inlets and absolute pressure at the outlet. Similarly, the concentration of two different species was set at 1 mol/m^3 at one inlet and zero at another inlet. Table 2 lists the material properties of working fluids water and ethanol such as density, dynamic viscosity, specific heat capacity ratio, thermal expansion, thermal diffusivity, etc.

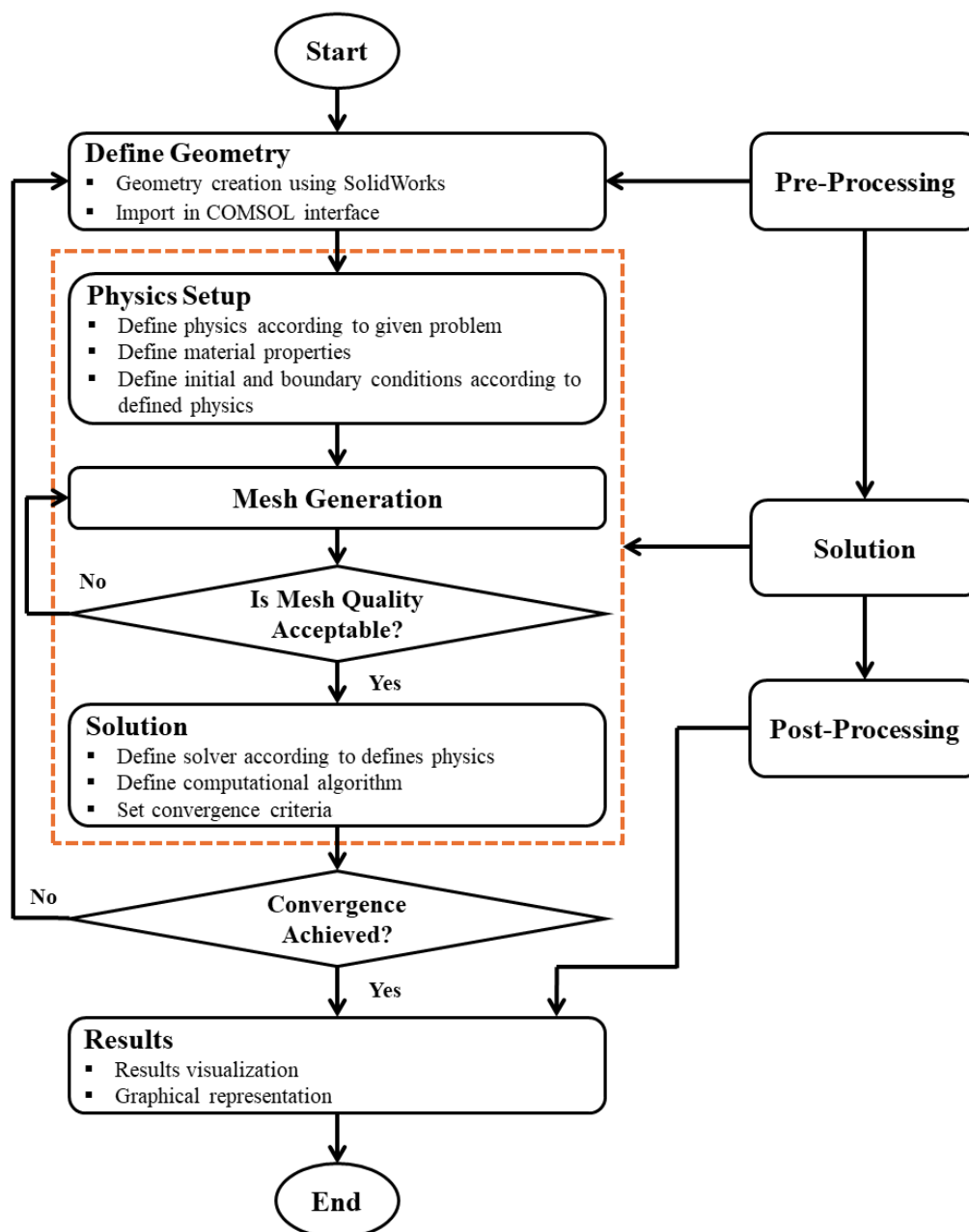


Figure 4. Numerical research methodology flowchart.

Table 2. Material properties of water and ethanol.

Properties	Water	Ethanol
Viscous dynamic viscosity	890 μ Pas	1200 μ Pas
Specific heat capacity	4180 J/KgK	2570 J/KgK
Density	997 Kg/m ³	789 Kg/m ³
Speed of sound	1497 m/s	1144 m/s
Compressibility	4.47×10^{-10} 1/Pa	1.1×10^{-9} 1/Pa
Specific heat capacity ratio	1.012	1.13
Thermal conductivity	0.61 W/mK	0.614 W/mK
Thermal expansion coefficient	2.74×10^{-4} 1/K	1.09×10^{-3} 1/K
Thermal diffusivity	1.464×10^{-7} m ² /s	7×10^{-8} m ² /s
Bulk dynamic viscosity	2.47 mPas	1.2 mPas

3. Mesh Independence Study

Optimal mesh density plays a crucial role in getting an accurate solution. Meanwhile, the accuracy of the solution, as well as computational cost, are greatly dependent on the number of elements in the mesh. In this research work, a mesh independence study is conducted at different refinement levels until a solution stability point is achieved. The details of different refinement levels are listed in Table 3. To examine the study of mesh independence, the mixing index is computed with different mesh refinement levels. Figure 5 describes the graphical representations of the mixing index with varying different levels of mesh refinement. The main goal of this mesh independence study is to determine the accuracy of the simulation solution. A mesh refinement level of 5 is used for the current study, and the total number of elements and nodes are 47,057 and 24,893, respectively, with an average value of skewness of 0.84. It can be clearly seen in Figure 5 that after the refinement level of 5, there is no major difference in the results. Thus, the mesh refinement level of 5 is considered the best mesh that lies within the acceptable range for current simulations considering the accuracy of the solution at appropriate computational cost.

Table 3. Description of the mesh independence study.

Mesh Refinement Level	Number of Elements	Number of Nodes	Mixing Index
1	32,797	17,762	0.760
2	36,760	19,744	0.711
3	38,622	20,675	0.783
4	41,444	22,086	0.798
5	47,057	24,893	0.820
6	60,397	31,563	0.821
7	76,933	39,831	0.821

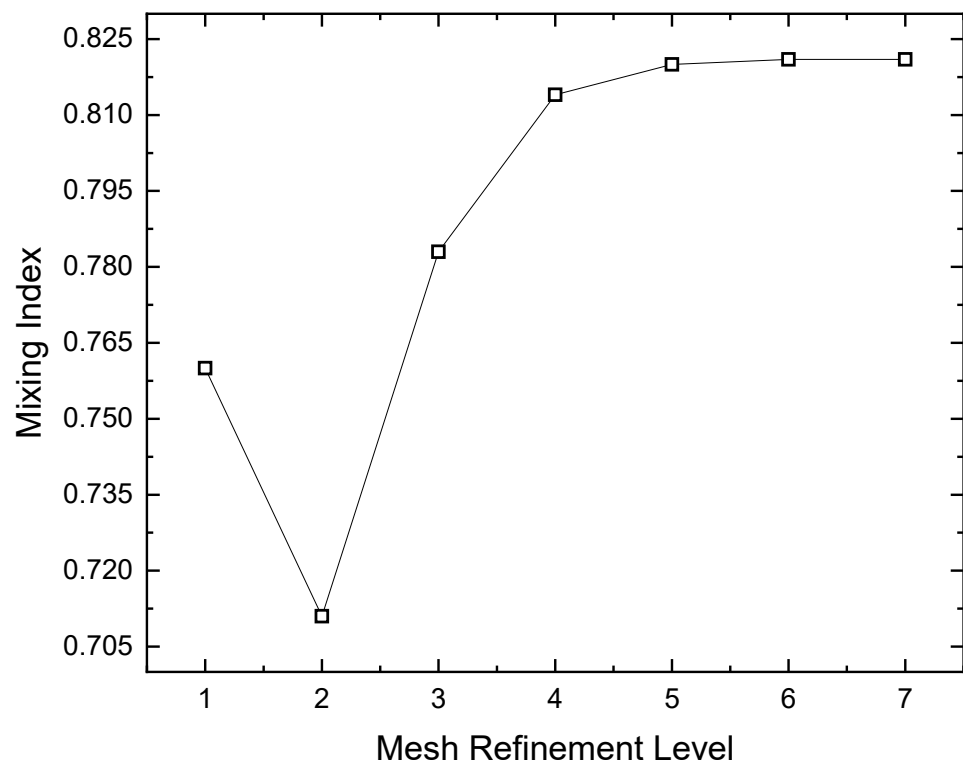


Figure 5. Variation of the mixing index with different mesh refinement levels.

4. Results and Discussion

This section describes the details of discussions on the numerical simulation outcomes such as the characteristics of acoustic field, acoustic streaming, and fluid mixing with different micropillar shapes and micropillar gaps and their impact on the mixing performance of hybrid microfluidics micromixers.

4.1. Acoustic Field

4.1.1. Effect of Micropillar Shapes

In this section, the characteristics of acoustic fields, such as acoustic pressure and acoustic velocity, are discussed for different micropillar shapes. Figure 6 represents the variation of the acoustic pressure and acoustic velocity for different micropillar shapes. It can be seen in the graphical representations that the presence of micropillars in the microchamber results in a significant increase in acoustic pressure and acoustic velocity. The maximum value of acoustic pressure and acoustic velocity can be observed for the presence of blade-shaped micropillars compared to other shapes. Similarly, the lowest value can be observed without micropillars. On the basis of these observations, it can be examined that micropillars increase the strength of the acoustic field, resulting in enhancing the mixing performance of the micromixer. Furthermore, the contours of the acoustic pressure and acoustic velocity are shown in Figures 7 and 8. It can be examined in Figure 7 that the acoustic excitation is more localised near the microchamber wall in the absence of micropillars, while with the addition of micropillars, the acoustic field provides more surface area and field strength near the micropillar wall. Similarly, the velocity field is also shown in Figure 8.

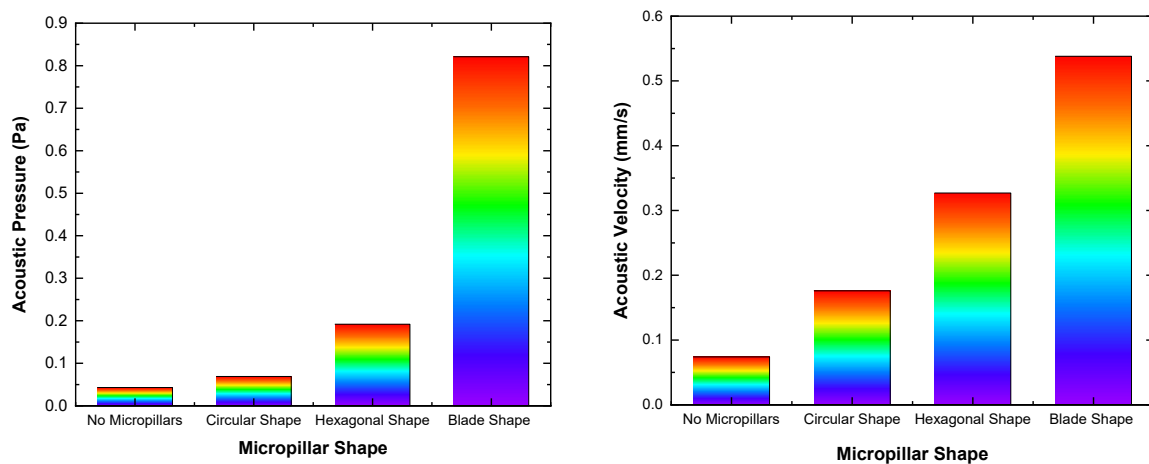


Figure 6. Graphical representation of the acoustic pressure and acoustic velocity with different micropillar shapes.

It is evident in Figure 8 that the presence of micropillars generates more streaming velocity near the micropillar wall, resulting in small vortices, which is helpful in enhancing the mixing performance. Higher streaming can be seen for the microchamber with blade-shaped micropillars. The maximum value of the acoustic field, such as acoustic pressure and acoustic velocity, is observed for blade-shaped micropillars compared to other micropillar shapes. Based on these observations, it can be examined that the inclusion of micropillars, especially the blade shape in the microchamber, can be significantly considered to intensify the mixing of two different heterogeneous fluids.

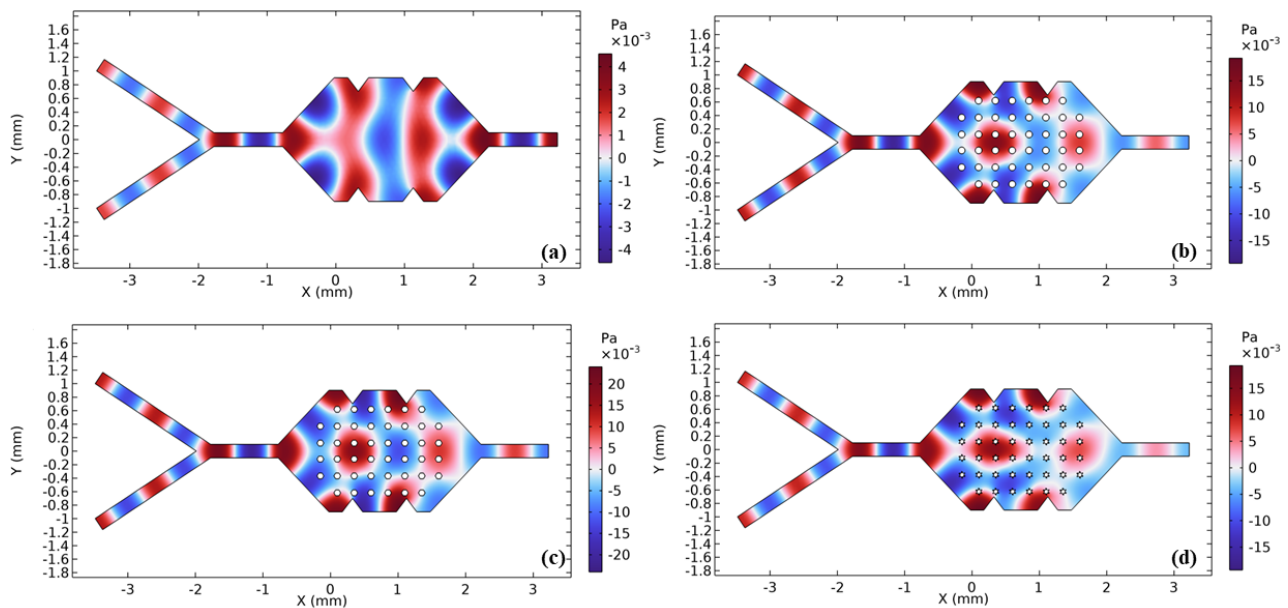


Figure 7. Acoustic pressure for different micropillar shapes: (a) no micropillars; (b) circular-shaped micropillars; (c) hexagonal-shaped micropillars; (d) blade-shaped micropillars.

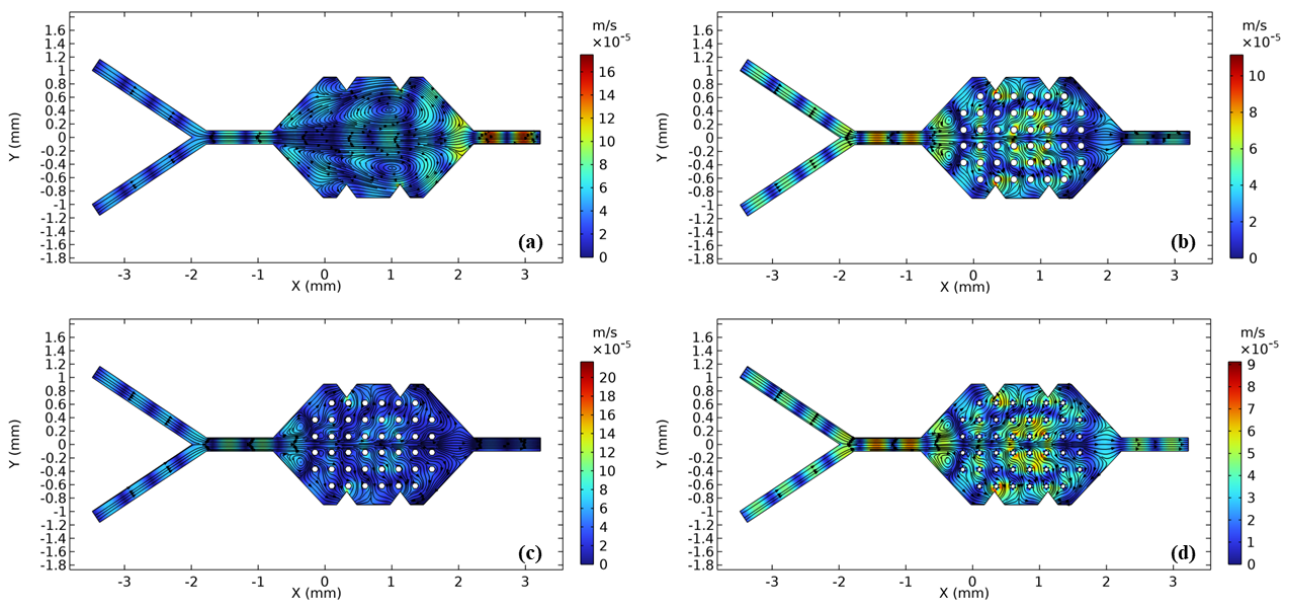


Figure 8. Acoustic velocity for different micropillars shapes: (a) no micropillars; (b) circular-shaped micropillars; (c) hexagonal-shaped micropillars; (d) blade-shaped micropillars.

4.1.2. Effect of Micropillar Gaps

This section describes the effect of micropillar gaps on acoustic fields, such as acoustic pressure and acoustic velocity. Figure 9 describes the graphical representations of the acoustic pressure and acoustic velocity with different micropillar gaps. It can be seen in the graphical representations that the acoustic pressure and acoustic velocity increased with the decrease in micropillar gaps. Furthermore, the blade-shaped micropillar has larger values of acoustic pressure and acoustic velocity than the other designs. Moreover, the maximum and minimum values of acoustic pressure and acoustic velocity are noted at micropillar gaps of 0.15 mm and 0.25 mm, respectively.

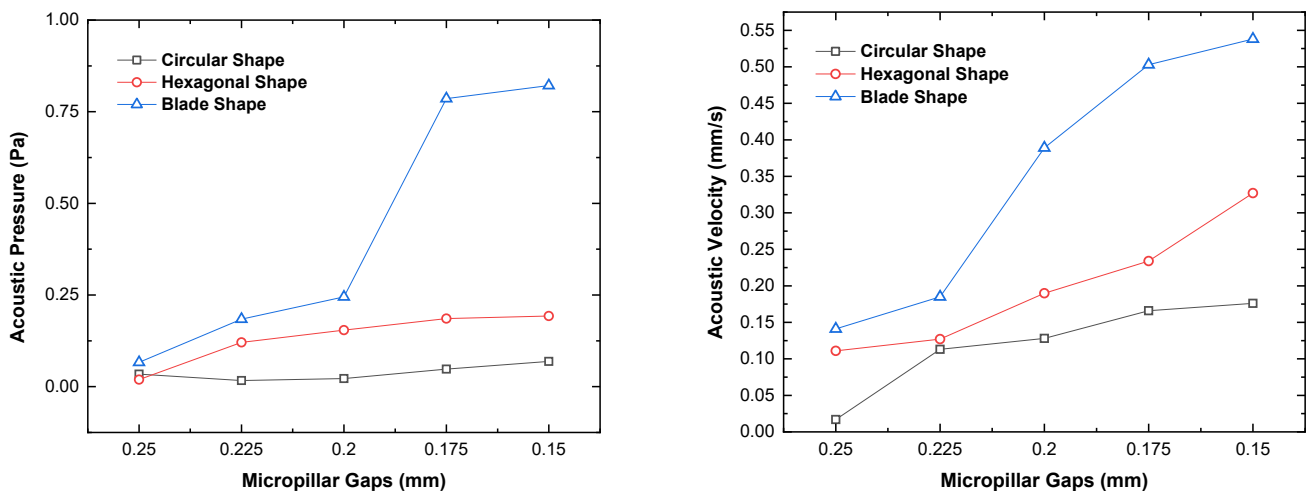


Figure 9. Variation of acoustic pressure and acoustic velocity with different micropillar gaps.

The main reason behind this increase in acoustic pressure and acoustic velocity with decreasing gaps is due to a larger surface area and more boundaries to hit. Thus, denser micropillars intensify the field strength, resulting in an enhancement of mixing performance. It was also noted that compared to the other micropillars, the blade-shaped micropillars with a 0.150 mm gap generate a stronger acoustic field and, according to the

computed results, the magnitude of acoustic pressure and acoustic velocity is approximately three and four times that of the case with no micropillars, respectively. The acoustic pressure and acoustic velocity distribution with different micropillar gaps are also shown in Figures 10 and 11.

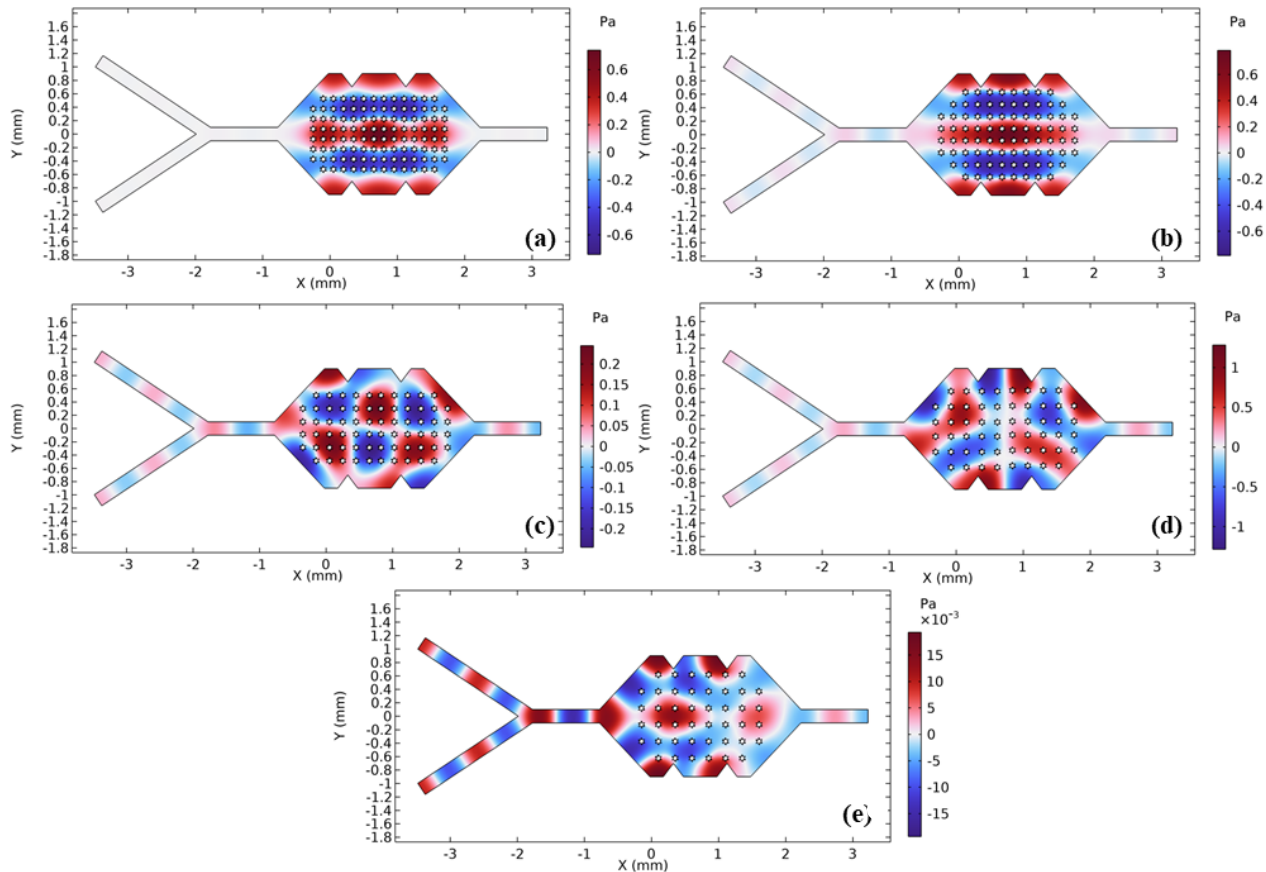


Figure 10. Distribution of acoustic pressure with different micropillar gaps: (a) 0.150 mm, (b) 0.175 mm, (c) 0.200 mm, (d) 0.225 mm, (e) 0.25 mm.

A stronger acoustic pressure field can be observed with a 0.150 mm micropillar gap compared to the others. Similarly, a less acoustic pressure field can be observed in the case of a 0.250 mm micropillar gap. The reason behind this higher field strength is because of a larger surface area and more boundaries to hit, which results in increasing the diffusion of fluids and mixing performance. The distribution of acoustic velocity can also be seen in Figure 11. Higher small vertices and acoustic velocity fields generated in the case of a 0.150 mm micropillar gap compared to the other cases. It can also be noted that fewer acoustic fields are generated near the wall in the case of a 0.150 mm gap compared to the other cases. The reason behind this strong acoustic field near the micropillars is due to a larger surface area and more boundaries in the microchamber than in the other cases.

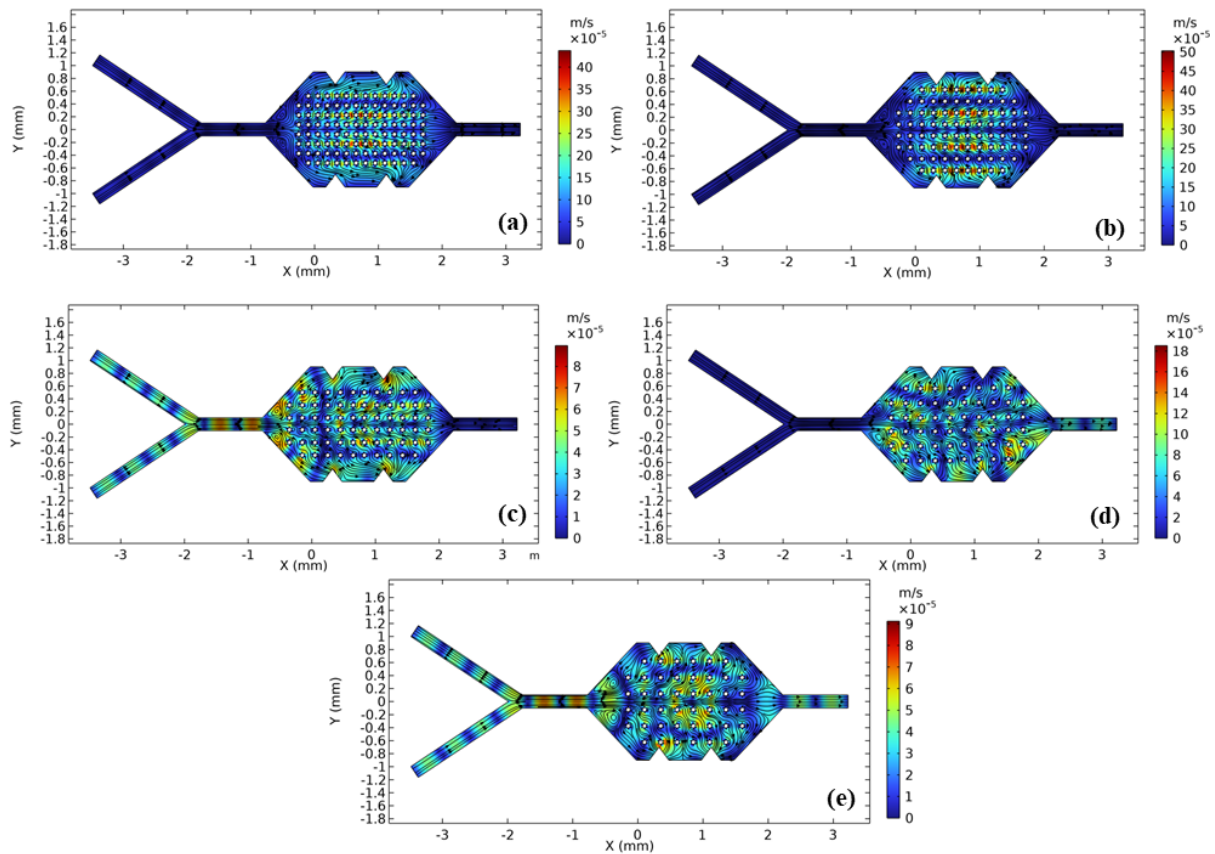


Figure 11. Distribution of acoustic velocity with different micropillar gaps: (a) 0.150 mm, (b) 0.175, mm (c) 0.200 mm, (d) 0.225 mm, (e) 0.25 mm.

4.2. Fluid Mixing

In this section, the fluid mixing phenomena with different micropillar shapes and micropillar gaps and their effect on mixing performance are discussed. Although the physics behind the mixing of two different heterogeneous fluids is entirely complicated, the degree of mixing can be quantified by measuring the degree of folding and stretching of fluids, as well as the simultaneous diffusion of species [49]. The process of stretching and folding in the case of two different heterogeneous fluids is followed by the collapse of stretched layers into smaller components, together with the simultaneous diffusion of species [50]. One of the key goals of this study is to intensify the mixing of two different heterogeneous fluids. The hybrid approach is one of the best ways to attain homogeneous mixing of two different heterogeneous fluids by employing acoustic streaming as an active approach and micropillars as a passive approach. The interfacial region near the wall of the micropillar is then significantly stretched and folded by intense microvortices that create lamellar structures. The mass diffusion rate of two different heterogeneous fluids intensifies due to the larger contact area in the presence of micropillars.

4.2.1. Effect of Micropillar Shapes

The quality of mixing can be quantified by determining the mixing index, which is given by Equations (1)–(3). Figure 12 shows the graphical representation of the variation of the mixing index for different micropillar shapes. Due to the hybrid approach and inclusion of micropillars, a higher mixing index can be observed compared to those without micropillars. In addition, among all shapes, the blade-shaped micropillars obtain a higher mixing index than the other shapes. The reason behind this higher mixing index is due to providing more contact area and boundaries in the case of blade-shaped micropillars compared to other cases. The concentration distribution of two different species can be seen

in Figure 13. It can be clearly observed that the maximum and minimum diffusion of species concentration are the cases of blade-shaped micropillars and no micropillars, respectively.

The magnitude of the mixing index for the cases of blade-shaped micropillars and no micropillars are 0.97 and 0.72, respectively. Because of the laminar flow nature of microfluidics systems, mixing occurs due to the diffusion of molecules. Thus, the inclusion of micropillars provides more contact area and generates more small vertices, resulting in enhancing the mixing performance. On the basis of the observations and computed findings, the presence of micropillars provide higher mixing performance.

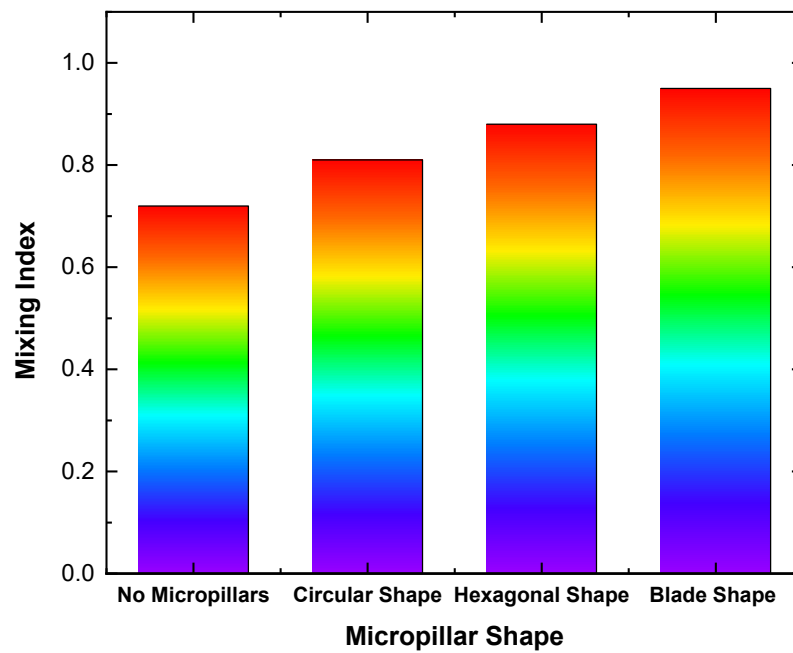


Figure 12. Variation of the mixing index for different micropillar shapes.

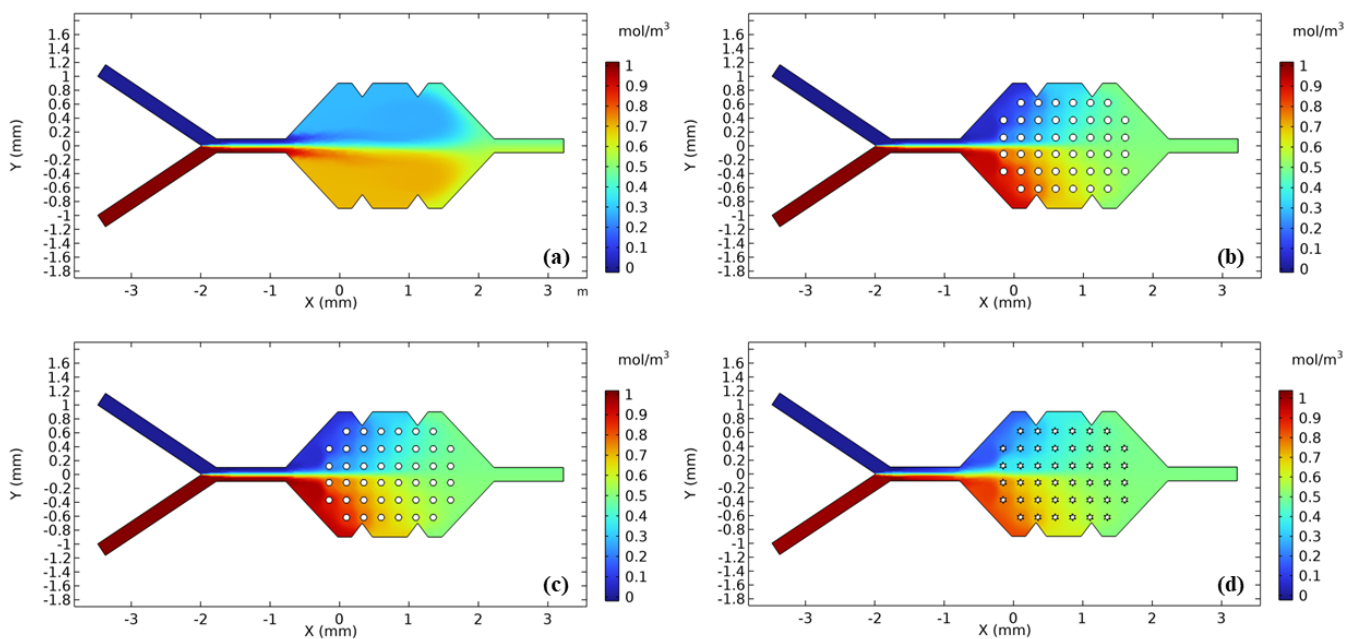


Figure 13. Distribution of species concentrations: (a) no micropillars, (b) circular micropillars, (c) hexagonal-shaped micropillars, (d) blade-shaped micropillars.

4.2.2. Effect of Micropillar Gaps

In this section, the effect of micropillar gaps on the mixing performance of microfluidic micromixers is investigated. Figure 14 represents the graphical representation of the variation of the mixing index by varying the micropillar gaps. It is evident that the mixing index increased linearly by decreasing the micropillar gaps. The higher mixing index can be observed for a 0.150 mm gap, while the lower mixing index can be observed for a 0.250 mm gap. The reason behind this larger value is due to the larger contact area and more boundaries to hit in the case of smaller micropillar gaps. On the other hand, among all micropillar shapes, the higher value of the mixing index can be noted in the case of blade-shaped micropillars. The reason behind this larger value in such a case is due to a larger contact area and intense microvortices near the micropillar walls compared to other shapes. Furthermore, the distribution of species concentrations with different micropillar gaps is also shown in Figure 15. The lower diffusion of species transports, as well as mixing, can be clearly observed in the case of a 0.250 mm micropillar gap. Similarly, a higher mixing and diffusion rate can be observed in the case of a 0.150 mm micropillar gap. The main reason behind this larger mixing index with small micropillar gaps is due to the larger contact area, resulting in generating more microvortices.

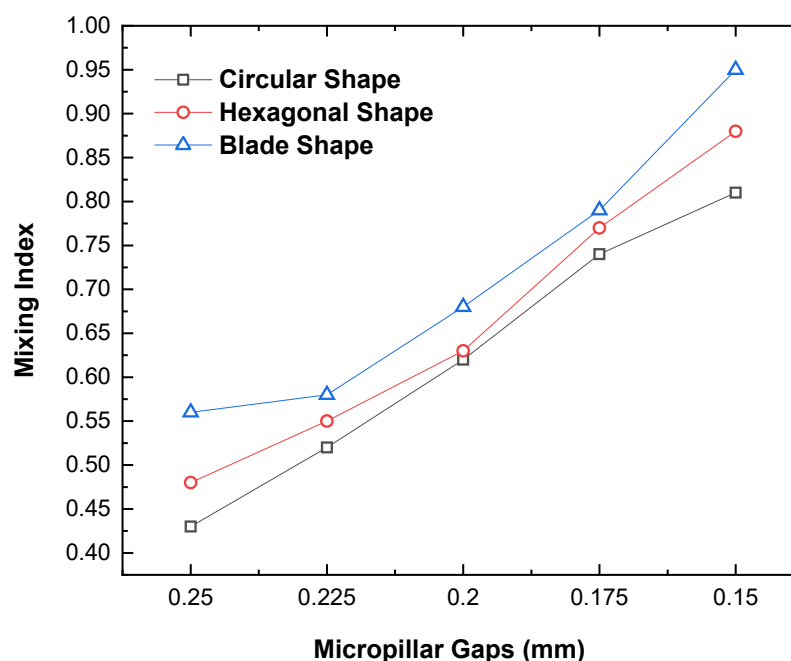


Figure 14. Variation of the mixing index with different micropillar gaps.

In a comparative examination of the performance of different micropillar shapes and micropillar gaps, it was investigated that the presence of micropillars in the microchamber of the microfluidics system is significant in improving the mixing performance of two different heterogeneous fluids. In addition, blade-shaped micropillars with a 0.150 mm gap deliver the best outcomes and perform better as compared to the other cases. As discussed earlier, this is due to employing a hybrid actuation approach and a higher diffusion rate of species concentrations. Finally, it is concluded that the proposed hybrid microfluidic micromixer can be used for high-quality mixing and reaction kinetics.

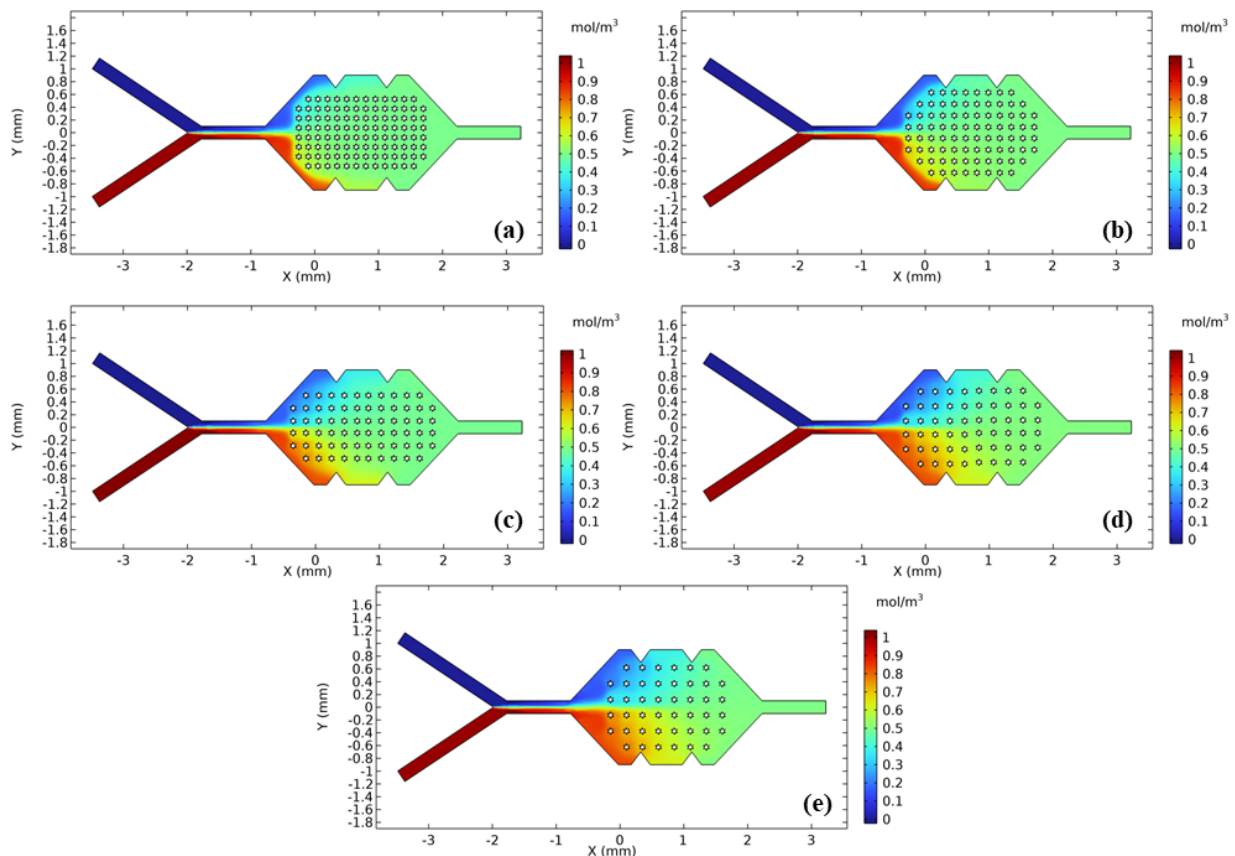


Figure 15. Distribution of species concentration with different micropillar gaps: (a) 0.150 mm, (b) 0.175 mm, (c) 0.200 mm, (d) 0.225 mm, (e) 0.25 mm.

4.3. Flow Field

Effect of Reynolds Number

This section describes the effect of various Reynolds numbers such as 2, 4, 6, 8, 10, and 12 on the mixing performance of microfluidic micromixers. Figure 16 describes the graphical representations of the variation of the mixing index by different Reynolds numbers. It can be observed that the mixing index decreased linearly with the Reynolds number, but non-linear behaviour has been noted for the case with no micropillars; at first, it increased, and then it decreased. The maximum mixing performance is observed at Reynolds number 2, while the minimum mixing performance is examined at Reynolds number 12. Similar behaviour has been observed in [51], where they investigated the maximum mixing performance index at Reynolds number 1×10^{-3} , corresponding to a flow velocity of 0.05 mm/s, and the lowest mixing performance index at 2×10^{-3} , corresponding to a flow velocity 0.1 mm/s. The main reason behind this linear decrease in mixing performance is the inclusion of micropillars, which help to properly homogenise the heterogeneous fluids in the microchamber. Moreover, the non-linear behaviour in the case of no micropillars is also observed due to improper mixing in the microchamber. Furthermore, the contours of distribution of flow velocity distribution at different Reynolds numbers of microfluidic micromixers are also presented in Figure 17. It can be observed that the maximum flow velocity is obtained at a Reynolds number of 12, while the lowest flow velocity is observed at a Reynolds number of 2. The maximum and minimum magnitudes of flow velocity are 0.00146 m/s and 2.58×10^{-4} m/s, respectively.

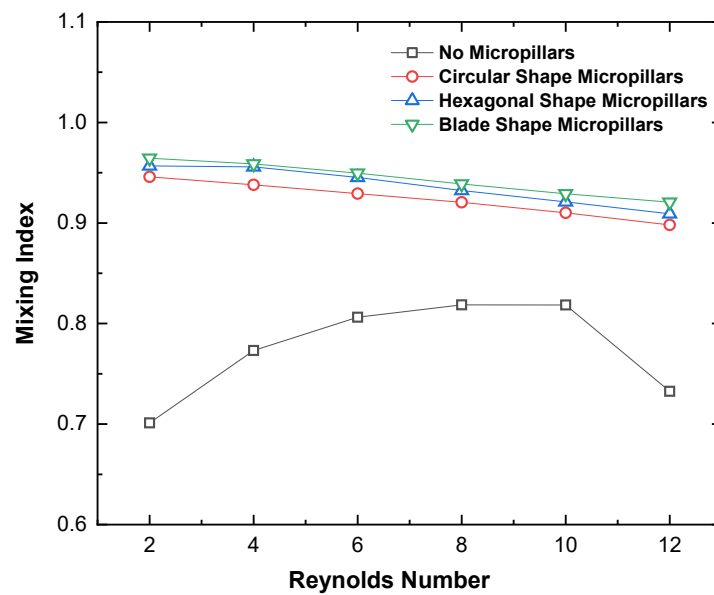


Figure 16. Graphical representations of the mixing index at different Reynolds numbers.

Moreover, streamlines in the case of the 12 Reynolds number is stronger compared to other values that cause a lower contact area and lower contact time for the mixing of different fluids, while lower Reynolds number values provide more contact area and contact time for the proper mixing of fluids. Finally, it is investigated that better mixing is observed at lower Reynolds numbers with fewer micropillar gaps for blade-shaped micropillars.

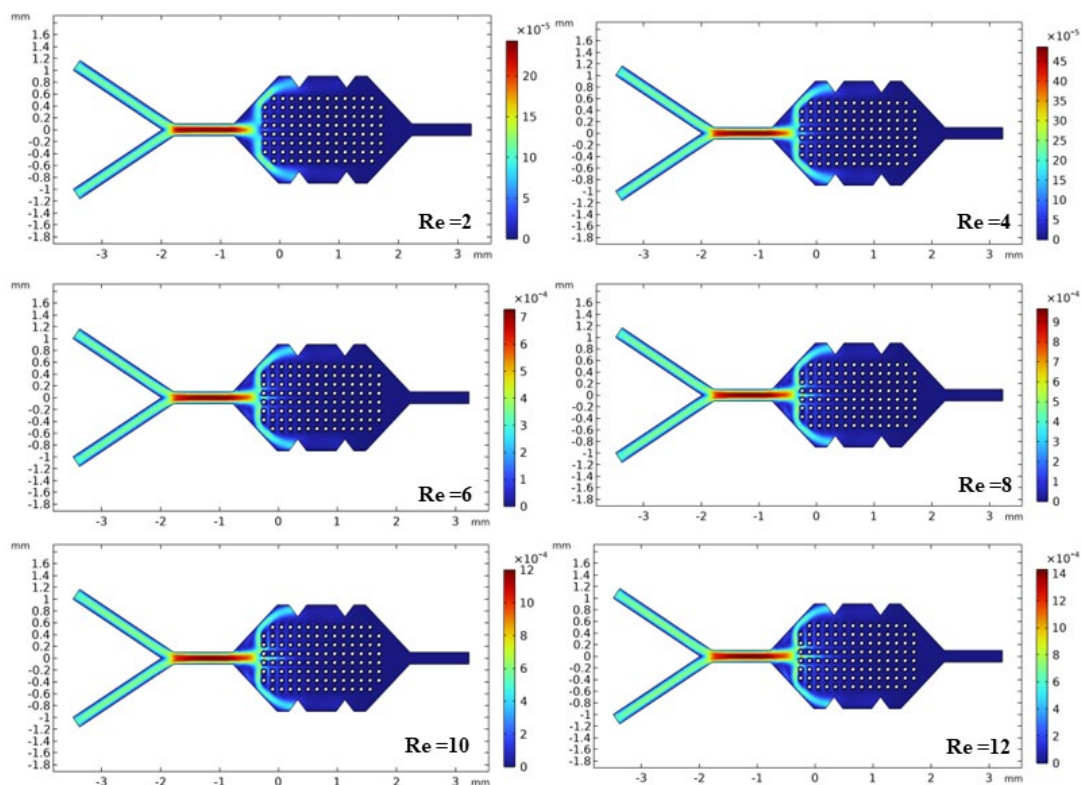


Figure 17. Distribution of the species concentration in different Reynolds numbers.

In addition, a comparison study has also been conducted in order to compare the mixing performance of the present work with the current literature on various microfluidic micromixers listed in Table 4. It is evident that people conducted performance analysis on various types of microfluidics micromixer designs, but the present proposed micromixer design has a better mixing index of 0.97. Furthermore, the mixing index can be improved based on these findings.

Table 4. Comparison study with the current literature.

Flow Rates/Re	Mixing Index	References
7.5×10^{-3} to 150×10^{-2}	0.96	[52]
0.1 to 100	0.85	[22]
$\leq 60 \mu\text{L}/\text{min}$	0.93	[23]
2 mL/min	0.89	[40]
2–12	0.97	Present Study

5. Conclusions

This paper investigated the performance of a microfluidic micromixer using a hybrid actuation approach, such as active (acoustic) and passive (inclusion of micropillars in the microfluidics chamber). The simulations were performed for four different micromixer designs such as circular-shaped micropillars, hexagonal-shaped micropillars, blade-shaped micropillars, and without micropillars. Additionally, different micropillar gaps such as 0.150 mm, 0.175 mm, 200 mm, 225 mm, and 250 mm were also used to investigate mixing performance. The detailed conclusions drawn from this study are described below.

1. The performance of microfluidics micromixers is greatly affected by the inclusion of micropillars compared to the case with no micropillars. The presence of micropillars in the microfluidic chamber increases the microvortices and strengthens the acoustic field.
2. Similarly, the shapes of micropillars are also impacted by the flow characteristics and the mixing performance of the microfluidic micromixer. Various micropillar shapes such as circular, hexagonal, and blade were investigated and compared to the case with no micropillars. The inclusion of blade-shaped micropillars delivers the best outcomes compared to the other shapes.
3. The performance of the microfluidic micromixer was also investigated with different micropillar gaps and found that the mixing performance increased with the decreasing of micropillar gaps. The reason behind this increment in performance is due to larger surface areas and more boundaries to generate higher microvortices and strengthen the acoustic field near the micropillar walls. The maximum performance was achieved with a micropillar gap of 0.150 mm.
4. It was also investigated that mixing performance and flow characteristics are significantly affected by altering the Reynolds numbers. It was revealed that the mixing performance increased with decreasing Reynolds numbers. The maximum and minimum values of mixing performance were achieved at Reynolds numbers of 2 and 12, respectively.
5. The maximum and minimum magnitude values of 0.97 and 0.70 for the mixing index are achieved, respectively, with the inclusion of blade-shaped micropillars and a 0.150 mm micropillar gap.
6. On the basis of the current research work, further work is required for the optimisation of hybrid microfluidics micromixers based on various micropillar arrangements. In addition, an analysis of the acoustic structure with different materials and geometrical parameters is also required to examine the structural stability and structural strength of the micropillars.

Author Contributions: Conceptualization, M.W. and G.J.; Methodology, A.P.; Software, M.W. and G.J.; Validation, G.J., V.N. and A.P.; Formal analysis, V.N. and A.P.; Investigation, M.W., G.J. and A.P.; Writing—original draft, M.W.; Writing—review & editing, G.J. and A.P. All authors have read and agreed to the published version of the manuscript.

Funding: This research received no external funding.

Institutional Review Board Statement: Not applicable.

Informed Consent Statement: Not Applicable.

Data Availability Statement: The data presented in this study are available in the article.

Conflicts of Interest: The authors declare no conflicts of interest.

References

1. Juraeva, M.; Kang, D.J. Mixing performance of a cross-channel split-and-recombine micro-mixer combined with mixing cell. *Micromachines* **2020**, *11*, 685. <https://doi.org/10.3390/mi11070685>.
2. Wan, T.; Wang, B.; Han, Q.; Chen, J.; Li, B.; Wei, S. A review of superhydrophobic shape-memory polymers: Preparation, activation, and applications. *Appl. Mater. Today* **2022**, *29*, 101665. <https://doi.org/10.1016/j.apmt.2022.101665>.
3. Prakash, S.; Kumar, S. Fabrication of microchannels: A review. *Proc. Inst. Mech. Eng. Part B J. Eng. Manuf.* **2015**, *229*, 1273–1288. <https://doi.org/10.1177/0954405414535581>.
4. Shi, S.; Abbas, Z.; Zheng, X.; Zhao, X.; Wang, D. Direct writing of suspended nanowires using coaxial electrohydrodynamic jet with double tip assistance. *J. Sol-Gel Sci. Technol.* **2024**, *110*, 1–14 <https://doi.org/10.1007/s10971-024-06454-1>.
5. Bahrami, D.; Nadooshan, A.A.; Bayareh, M. Effect of non-uniform magnetic field on mixing index of a sinusoidal micromixer. *Korean J. Chem. Eng.* **2022**, *39*, 316–327. <https://doi.org/10.1007/s11814-021-0932-z>.
6. Lee, B.; Kim, M.; Oh, S.; Bi Lee, D.; Lee, S.G.; Min Kim, H.; Kim, K.H.; Song, J.; Lee, C.S. Characterization of passive microfluidic mixer with a three-dimensional zig-zag channel for cryo-EM sampling. *Chem. Eng. Sci.* **2023**, *281*, 119161. <https://doi.org/10.1016/j.ces.2023.119161>.
7. Tripathi, E.; Patowari, P.K.; Pati, S. Numerical investigation of mixing performance in spiral micromixers based on Dean flows and chaotic advection. *Chem. Eng. Process.-Process Intensif.* **2021**, *169*, 108609. <https://doi.org/10.1016/j.cep.2021.108609>.
8. Bai, C.; Zhou, W.; Yu, S.; Zheng, T.; Wang, C. A surface acoustic wave-assisted micromixer with active temperature control. *Sens. Actuators A Phys.* **2022**, *346*, 113833. <https://doi.org/10.1016/j.sna.2022.113833>.
9. Li, Z.; Zhang, B.; Dang, D.; Yang, X.; Yang, W.; Liang, W. A review of microfluidic-based mixing methods. *Sens. Actuators A Phys.* **2022**, *344*, 113757. <https://doi.org/10.1016/j.sna.2022.113757>.
10. Husain, A.; Khan, A.I.; Raza, W.; Al-Rawahi, N.; Al-Azri, N.; Samad, A. Design and Mixing Performance of Passive Micromixers: A Critical Review. *J. Eng. Res.* **2023**, *19*, 106–128. <https://doi.org/10.53540/TJER.VOL19ISS2PP106-128>.
11. Kumar, C.; Hejazian, M.; From, C.; Saha, S.C.; Sauret, E.; Gu, Y.; Nguyen, N.T. Modeling of mass transfer enhancement in a magnetofluidic micromixer. *Phys. Fluids* **2019**, *31*, 063603. <https://doi.org/10.1063/1.5093498>.
12. Rahimi, M.; Aghel, B.; Hatamifar, B.; Akbari, M.; Alsairafi, A.A. CFD modeling of mixing intensification assisted with ultrasound wave in a T-type microreactor. *Chem. Eng. Process. Process Intensif.* **2014**, *86*, 36–46. <https://doi.org/10.1016/j.cep.2014.10.006>.
13. Jalili, H.; Raad, M.; Fallah, D.A. Numerical study on the mixing quality of an electroosmotic micromixer under periodic potential. *Proc. Inst. Mech. Eng. Part C J. Mech. Eng. Sci.* **2020**, *234*, 2113–2125. <https://doi.org/10.1177/0954406220904089>.
14. Gong, Y.; Cheng, X. Numerical investigation of electroosmotic mixing in a contraction–expansion microchannel. *Chem. Eng. Process.-Process Intensif.* **2023**, *192*, 109492. <https://doi.org/10.1016/j.cep.2023.109492>.
15. Xiong, S.; Chen, X.; Chen, H.; Chen, Y.; Zhang, W. Numerical study on an electroosmotic micromixer with rhombic structure. *J. Dispers. Sci. Technol.* **2021**, *42*, 1331–1337. <https://doi.org/10.1080/01932691.2020.1748644>.
16. Mondal, B.; Mehta, S.K.; Pati, S.; Patowari, P.K. Numerical analysis of electroosmotic mixing in a heterogeneous charged micromixer with obstacles. *Chem. Eng. Process.-Process Intensif.* **2021**, *168*, 108585. <https://doi.org/10.1016/j.cep.2021.108585>.
17. Vasista, K.N.; Mehta, S.K.; Pati, S. Electroosmotic mixing in a microchannel with heterogeneous slip dependent zeta potential. *Chem. Eng. Process.-Process Intensif.* **2022**, *176*, 108940. <https://doi.org/10.1016/j.cep.2022.108940>.
18. Tata Rao, L.; Goel, S.; Kumar Dubey, S.; Javed, A. Performance Investigation of T-Shaped Micromixer with Different Obstacles. *J. Phys. Conf. Ser.* **2019**, *1276*, 012003. <https://doi.org/10.1088/1742-6596/1276/1/012003>.
19. Green, J.; Holdø, A.; Khan, A. A review of passive and active mixing systems in microfluidic devices. *Int. J. Multiphys.* **2007**, *1*, 1–32. <https://doi.org/10.1260/175095407780130544>.
20. Farahinia, A.; Zhang, W.J. Numerical investigation into the mixing performance of micro T-mixers with different patterns of obstacles. *J. Braz. Soc. Mech. Sci. Eng.* **2019**, *41*, 491. <https://doi.org/10.1007/s40430-019-2015-1>.
21. Xia, A.; Shen, C.; Wei, C.; Meng, L.; Hu, Z.; Zhang, L.; Chen, M.; Li, L.; He, N.; Hao, X. Numerical and Experimental Investigation on a “Tai Chi”-Shaped Planar Passive Micromixer. *Micromachines* **2023**, *14*, 1414. <https://doi.org/10.3390/mi14071414>.
22. Jiang, Y.; Zhang, Y. High performance micromixers by 3D printing based on split-and-recombine modules and twisted-architecture microchannel. In Proceedings of the 5th International Conference on Intelligent Human Systems Integration (IHSI 2022): Integrating People and Intelligent Systems, Venice, Italy, 22–24 February 2022; Volume 22. <https://doi.org/10.54941/ahfe1001085>.

23. Wang, Z.; Yan, X.; Zhou, Q.; Wang, Q.; Zhao, D.; Wu, H. A Directly Moldable, Highly Compact, and Easy-for-Integration 3D Micromixer with Extraordinary Mixing Performance. *Anal. Chem.* **2023**, *95*, 8850–8858. <https://doi.org/10.1021/acs.analchem.3c00335>.
24. Shao, Y.; Wang, H.; Zhang, Q.; Xie, Z.; Zhu, X.; Ding, Y.; Chen, R.; Liao, Q. Cross-channel microfluidic device for dynamic control of concentration and velocity by the electroosmotic drive. *Chem. Eng. Sci.* **2023**, *281*, 119139. <https://doi.org/10.1016/j.ces.2023.119139>.
25. Ward, K.; Fan, Z.H. Mixing in microfluidic devices and enhancement methods. *J. Micromechanics Microengineering* **2015**, *25*, 094001. <https://doi.org/10.1088/0960-1317/25/9/094001>.
26. You, J.B.; Kang, K.; Tran, T.T.; Park, H.; Hwang, W.R.; Kim, J.M.; Im, S.G. PDMS-based turbulent microfluidic mixer. *Lab Chip* **2015**, *15*, 1727–1735. <https://doi.org/10.1039/c5lc00070j>.
27. Chen, X.; Lv, H. New insights into the micromixer with Cantor fractal obstacles through genetic algorithm. *Sci. Rep.* **2022**, *12*, 4162. <https://doi.org/10.1038/s41598-022-08144-w>.
28. Xiong, M.; Yang, J.; Ding, X.; Li, H.; Zhang, H. Topology optimization design of micromixer based on principle of Tesla valve: An experimental and numerical study. *Chem. Eng. Process.-Process Intensif.* **2023**, *193*, 109560. <https://doi.org/10.1016/j.cep.2023.109560>.
29. Chen, Z.; Pei, Z.; Zhao, X.; Zhang, J.; Wei, J.; Hao, N. Acoustic microreactors for chemical engineering. *Chem. Eng. J.* **2022**, *433*, 133258. <https://doi.org/10.1016/j.cej.2021.133258>.
30. Ahmed, H.; Park, J.; Destgeer, G.; Afzal, M.; Sung, H.J. Surface acoustic wave-based micromixing enhancement using a single interdigital transducer. *Appl. Phys. Lett.* **2019**, *114*, 043702. <https://doi.org/10.1063/1.5079815>.
31. Lim, H.; Back, S.M.; Choi, H.; Nam, J. Acoustic mixing in a dome-shaped chamber-based SAW (DC-SAW) device. *Lab Chip* **2020**, *20*, 120–125. <https://doi.org/10.1039/c9lc00820a>.
32. Li, X.; Huffman, J.; Ranganathan, N.; He, Z.; Li, P. Acoustofluidic enzyme-linked immunosorbent assay (ELISA) platform enabled by coupled acoustic streaming. *Anal. Chim. Acta* **2019**, *1079*, 129–138. <https://doi.org/10.1016/j.aca.2019.05.073>.
33. Lee, C.; Chang, C.; Yang, Y.; Fu, L. *Microfluidic Mixing*; Springer: Berlin/Heidelberg, Germany, 2011; pp. 1–13, Volume 12. https://doi.org/10.1007/springerreference_67173.
34. Gharib, G.; Bütün, İ.; Muganlı, Z.; Kozalak, G.; Namlı, İ.; Sarraf, S.S.; Ahmadi, V.E.; Toyran, E.; van Wijnen, A.J.; Koşar, A. Biomedical Applications of Microfluidic Devices: A Review. *Biosensors* **2022**, *12*, 1023. <https://doi.org/10.3390/bios12111023>.
35. Francesko, A.; Cardoso, V.F.; Lanceros-Méndez, S. Lab-on-a-chip technology and microfluidics. In *Microfluidics for Pharmaceutical Applications*; Elsevier: Amsterdam, The Netherlands, 2019; ISBN 9780128126592. <https://doi.org/10.1016/B978-0-12-812659-2.00001-6>.
36. Khan, M.A.; Suhaib, M.; Ansari, M.A. Investigations on fluid flow and mixing in fractal tree like biomimetic microchannel based on Murray's law. *Chem. Eng. Process.-Process Intensif.* **2023**, *194*, 109564. <https://doi.org/10.1016/j.cep.2023.109564>.
37. Liu, F.; Zhang, J.; Alici, G.; Yan, S.; Mutlu, R.; Li, W.; Yan, T. An inverted micro-mixer based on a magnetically-actuated cilium made of Fe doped PDMS. *Smart Mater. Struct.* **2016**, *25*, 095049. <https://doi.org/10.1088/0964-1726/25/9/095049>.
38. Le, P.T.; An, S.H.; Jeong, H. Microfluidic Tesla mixer with 3D obstructions to exceptionally improve the curcumin encapsulation of PLGA nanoparticles. *Chem. Eng. J.* **2024**, *483*, 149377. <https://doi.org/10.1016/j.cej.2024.149377>.
39. Kim, W.; Cha, B.; Jeon, J.S.; Park, J. Acoustofluidic control of chemical concentration within picoliter droplets in a disposable microfluidic chip. *Sens. Actuators B Chem.* **2023**, *393*, 134132. <https://doi.org/10.1016/j.snb.2023.134132>.
40. Wang, J.; Cui, B.; Liu, H.; Chen, X.; Li, Y.; Wang, R.; Lang, T.; Yang, H.; Pan, H.; Quan, J.; et al. Tesla Valve-Based Flexible Microhybrid Chip with Unidirectional Flow Properties. *ACS Omega* **2022**, *7*, 31744–31755. <https://doi.org/10.1021/acsomega.2c02075>.
41. Juraeva, M.; Kang, D. Mixing Performance of the Modified Tesla Micromixer with Tip Clearance. *Micromachines* **2022**, *13*, 1375.
42. Jalilvand, E.; Shamloo, A.; Gangaraj, M.H. Computational study of an integrated microfluidic device for active separation of RBCs and cell lysis. *Chem. Eng. Process.-Process Intensif.* **2022**, *174*, 108891. <https://doi.org/10.1016/j.cep.2022.108891>.
43. Pawinanto, R.E.; Yunas, J.; Hashim, A.M. Design optimization of active microfluidic mixer incorporating micropillar on flexible membrane. *Microsyst. Technol.* **2019**, *25*, 1203–1209. <https://doi.org/10.1007/s00542-018-4134-5>.
44. Hong, C.C.; Choi, J.W.; Ahn, C.H. A novel in-plane passive microfluidic mixer with modified Tesla structures. *Lab Chip* **2004**, *4*, 109–113. <https://doi.org/10.1039/b305892a>.
45. Bruus, H. Acoustofluidics 1: Governing equations in microfluidics. *Lab Chip* **2011**, *11*, 3742–3751. <https://doi.org/10.1039/c1lc20658c>.
46. Bruus, H. *Theoretical Microfluidics*; Oxford Academic: New York, NY, USA, 1997; ISBN 9780199235087. <https://doi.org/10.1093/oso/9780199235087.001.0001>.
47. Bruus, H. Governing Equations in Microfluidics. In *Microscale Acoustofluidics*; Royal Society of Chemistry: Cambridge, UK, 2014; pp. 1–28.
48. Novoselac, A. Chapter 18. Theory. 2002; Volume 0, pp. 1–52. [Online]. Available: http://www.ce.utexas.edu/prof/Novoselac/classes/ARE372/handouts/CFD_theory.pdf (accessed on 20 December 2023).
49. Ottino, J.M. The Kinematics of Mixing: Stretching, Chaos and Transport. In *Cambridge Texts in Applied Mathematics*; Cambridge University Press: Cambridge, UK, 2004. [Online]. Available: <https://books.google.lt/books?id=8OLVcbRoNSgC&lpq=PP1&hl=lt&pg=PP1#v=onepage&q&f=false> (accessed on 14 November 2023).
50. Barman, C.; Bandopadhyay, A. Mixing intensification in an acoustofluidic micromixer aided with micro-pillars. *Chem. Eng. Process.-Process Intensif.* **2023**, *194*, 109604. <https://doi.org/10.1016/j.cep.2023.109604>.

51. Agarwal, A.; Salahuddin, A.; Wang, H.; Ahamed, M.J. Design and development of an efficient fluid mixing for 3D printed lab-on-a-chip. *Microsyst. Technol.* **2020**, *26*, 2465–2477. <https://doi.org/10.1007/s00542-020-04787-9>.
52. Chen, Z.; Wang, Y.; Zhou, S. Numerical Analysis of Mixing Performance in an Electroosmotic Micromixer with Cosine Channel Walls. *Micromachines* **2022**, *13*, 1933. <https://doi.org/10.3390/mi13111933>.

Disclaimer/Publisher’s Note: The statements, opinions and data contained in all publications are solely those of the individual author(s) and contributor(s) and not of MDPI and/or the editor(s). MDPI and/or the editor(s) disclaim responsibility for any injury to people or property resulting from any ideas, methods, instructions or products referred to in the content.